CMNE/CILAMCE 2007
Porto, 13-15 Junho, 2007

APPLICATION OF FLUX-CORRECTED TRANSPORT TO AN UNSTRUCTURED-GRID FINITE-VOLUME FORMULATION FOR RESERVOIR SIMULATION

Fernando S. V. Hurtado, Clovis R. Maliska and Antonio F. C. da Silva

SINMEC - Computational Fluid Dynamics Lab
Mechanical Engineering Department
Federal University of Santa Catarina
88040-900, Campus Universitário, Florianópolis / SC, Brazil
e-mail: fernando@sinmec.ufsc.br, maliska@sinmec.ufsc.br, afabio@sinmec.ufsc.br
web: http://www.sinmec.ufsc.br

Keywords: Reservoir simulation, numerical diffusion, high-resolution schemes.

Summary. *In this work, the flux-corrected transport (FCT) technique is applied to a finite-volume reservoir flow numerical model, in order to reduce numerical diffusion near discontinuities maintaining solutions free of oscillations and other numerical artifacts. This simple and powerful technique is based on flux limiters that switch between low-order and high-order approximations depending on the smoothness of the solution. While in smooth regions the high-order approximation is maintained, near discontinuities positivity constraints are invoked in order to impose flux restrictions that prevent the formation of nonphysical oscillations. Since actual reservoirs exhibit complex geometries and intricate geological features that only can be represented accurately with unstructured grids, all developments considered in this work are based in a numerical formulation capable of dealing with this type of grids. This formulation employs the element-based finite-volume method (EbFVM) for discretizing the differential equations that describes multiphase flow in reservoirs.*

1. INTRODUCTION

Nowadays, most of commercial reservoir simulators are still based on the first-order single-point upstream scheme for the approximation of advection terms. Simplicity and robustness matters are generally argued as the main reasons for the persistence of this scheme. Nevertheless, it is well-known that the use single-point upstream schemes introduces high levels of numerical diffusion that strongly smear front discontinuities generally present in reservoir flow solutions [1] [2] [14]. This smearing frequently causes several inaccurate predictions, for example, the prediction of early breakthrough times for waterflood processes. The single-point upstream scheme is also closely related with another numerical issue in reservoir simulation: the grid orientation effect [3]. As upstream value is usually determined between the values of two nodes joined by a grid line, a strong dependence on the local orientation of the grid is created using the single-point scheme.

Early attempts to reduce numerical diffusion in reservoir simulation included two-point upstream [18] and other second-order schemes [1]. Although these schemes are formally more accurate than the single-point scheme, it is not possible to guarantee that they will produce numerical solutions free of spurious oscillations and overshoots/undershoots near discontinuities [1] [14]. This situation is much more harmful than numerical diffusion because, besides of being totally unphysical, oscillations can produce unbounded values for always-positive magnitudes like concentration or saturation. A similar dichotomy between numerical diffusion and spurious oscillations is found in the simulation of compressible flow and other physical phenomena described by hyperbolic equations. The scientific community working in those areas developed several numerical techniques, collectively known as high-resolution schemes, for addressing the task of increasing the accuracy of first-order solutions, preventing at the same time the formation of oscillations in the neighborhood of discontinuities [7]. The basic idea behind those schemes is the switching between high-order approximations in smooth regions of the solution and first-order in regions of steep gradients and discontinuities. Since that operation requires information about the solution at a given time level, high-resolution schemes are necessarily nonlinear [7].

Some high-resolution schemes have been applied to reservoir simulation (see, for instance, references [3] [4] [5] [15]). To our knowledge, all of them were applied to one and/or two-dimensional problems discretized by Cartesian grids, since most of the high-resolution schemes were developed considering exclusively for that type of grids. Until now, it is not completely clear which is the best way for extending these schemes to unstructured grids.

Flux-corrected transport (FCT) is one of the high-resolution schemes more amenable to adaptation to an unstructured framework. For this reason, we have chosen FCT as the first alternative for including a high-resolution scheme into a finite-volume formulation developed for simulating multiphase flow in reservoirs discretized with unstructured grids. Currently, this type of grids is being gradually adopted in reservoir simulation, because actual petroleum reservoirs frequently exhibit such complex geometries and intricate geological features that only can be represented accurately with unstructured grids. The basic FCT technique is based on the correction of low-order monotonic solutions by means of antidiffusive fluxes computed in a way that a high-order solution would be obtained after correction. However, those antidiffusive fluxes are limited to an extent that prevents the introduction of new local extrema into the solution [10]. Flux limiters are usually determined employing the *local extremum diminishing* (LED) criterion,

which is a multidimensional generalization of the well-known *total variation diminishing* (TVD) criterion [11].

The paper is organized as follows. In section 2 we briefly describe our basis formulation for two-dimensional reservoir simulation using unstructured grids. This formulation is basically an application of the element-based finite-volume method (EbFVM) to the discretization of the differential equations modeling multiphase flow in porous media. Section 3 describes the implementation of the FCT strategy into the numerical formulation. Following, in section 4 are presented application examples showing the capability of the FCT for reducing numerical diffusion, employing the formulation just described. Finally, some concluding remarks are drawn in section 5.

2. THE ELEMENT-BASED FINITE-VOLUME BASIS FORMULATION

For the sake of simplicity, we consider a two-phase incompressible and immiscible flow model, neglecting any influence of capillary pressure. The numerical techniques introduced later for improving the quality of solutions can be transplanted straightforwardly to a more general formulation. The mathematical model for that kind of flow can be reduced to a pair of differential equations [1] [14], the so-called Buckley-Leverett form of the saturation equation,

$$\phi\, \partial_t s \; + \; \vec{\nabla} \cdot (F\, \vec{\mathbf{v}}_T) \; = \; 0 \,, \tag{1}$$

and the pressure differential equation,

$$\vec{\nabla} \cdot (\lambda_T \vec{\vec{\mathbf{K}}} \cdot \vec{\nabla} P) \; = \; 0 \,. \tag{2}$$

Here, ϕ and $\vec{\vec{\mathbf{K}}}$ are the porosity and the tensor of absolute permeability of the medium, respectively. The main variables on each equation are the saturation of water s and the pressure P. Furthermore, $\lambda_T = \lambda_w + \lambda_o$ is the total mobility (w stands for water phase and o stands for oil phase), and $F = \lambda_w / \lambda_T$ is known as fractional flux function, all of them being functions of the saturation. Finally, $\vec{\mathbf{v}}_T = \vec{\mathbf{v}}_w + \vec{\mathbf{v}}_o$ is the total velocity, a variable that couples the pressure and saturation equations, since it can be expressed as [14]

$$\vec{\mathbf{v}}_T \; = \; -\lambda_T \vec{\vec{\mathbf{K}}} \cdot \vec{\nabla} P \,. \tag{3}$$

In order to discretize in space the system of differential equations, the element-based finite-volume method (EbFVM) will be considered. This approach follows the basic guidelines of the conventional finite-volume method, namely the integration of differential equations over control volumes in a way that conservation is automatically enforced. However, a significant improvement in flexibility is introduced through the concept of element as the basic geometrical entity for the discretization of the solution domain, since in this way the use of unstructured grids is readily affordable. Here we only give a very brief introduction to the application of EbFVM, more details can be found elsewhere [8] [9] [13] [16].

The main geometric entities considered in EbFVM are shown in Fig. 1. The grid is formed by *elements*, which are quadrilateral in this work, they could be triangular also. These entities are used for defining the discretized geometry of the solution domain as well as for defining the

spatial variation of physical properties of the medium. The unknowns of the problem are calculated at the *nodes*, located at every element corner. Around every node is built a *control volume*, formed by portions of the elements sharing a common node. Every control volume is delimited by a certain number of *faces*, obtained joining the center of every neighboring element with the midpoint of its two sides sharing the node around which the control volume is built. Normally, a discretized equation for a control volume represents some kind of balance, thus, it becomes necessary to compute fluxes across the faces. As surface integrals defining fluxes are usually approximated by the midpoint rule, the face center points are also important entities in EbFVM and they are commonly known as *integration points*.

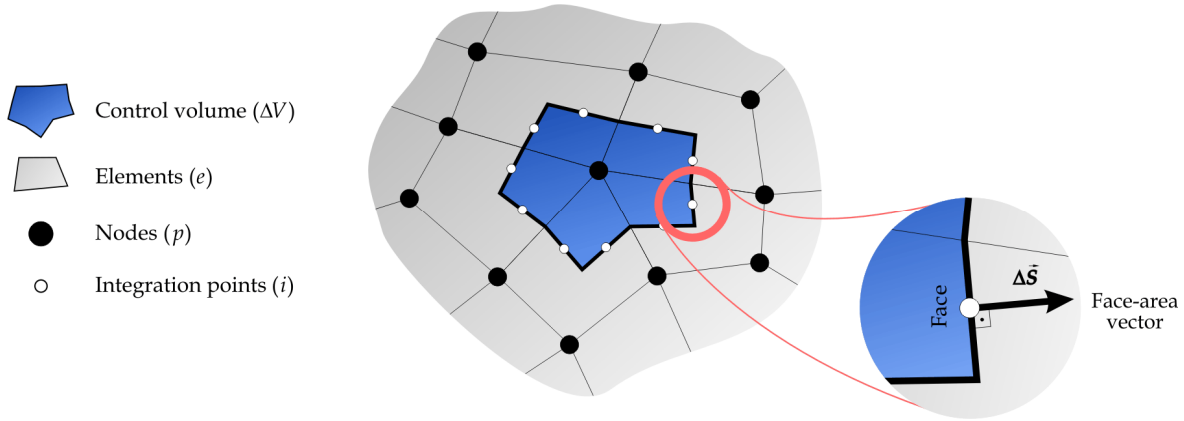

Figure 1 - Main geometrical entities on the element-based finite-volume method.

After integration of differential equations (1) and (2) over a generic control volume, they can be approximated, respectively, as

$$\frac{s_p^{n+1} - s_p^n}{\Delta t}\phi_p \Delta V_p + \sum_e \left\{ \sum_i F_i^n (\vec{\mathbf{v}}_T)_i^n \cdot \Delta \vec{\mathbf{S}}_i \right\}_e = 0\,, \tag{4}$$

$$\sum_e \left\{ \sum_i (\lambda_T)_i^n \left[\vec{\vec{\mathbf{K}}}_e \cdot (\vec{\nabla} P)_i^n \right] \cdot \Delta \vec{\mathbf{S}}_i \right\}_e = 0\,. \tag{5}$$

Here, subscripts specify the geometrical entities to which variables are related and superscripts specify the time level. A forward Euler approximation was considered for discretization in time while the mid-point rule was applied for approximating surface integrals at control volume faces. In Eqs. (4) and (5), ΔV_p is the volume of the control volume, $\Delta \vec{\mathbf{S}}_i$ is the area vector of a face limiting the control volume, $\vec{\vec{\mathbf{K}}}_e$ is the permeability tensor (constant inside an element) and Δt is the time-step. The outer summations involve all elements contributing to the control volume. On the other hand, the inner summations involve solely the two integration points that lies over the control volume faces inside a contributing element. For more details concerning to the EbFVM discretization process, see reference [8].

The forward Euler time approximation leads to the well-known IMPES approach [1] [14] for solving the discretized equations. This solution scheme is utilized in this work, since is the most straightforward way of introducing a flux-corrected transport strategy into the formulation. Another solution approach, such as the fully implicit scheme, could be considered also, though. The time approximation considered in IMPES decouples the pressure equation from the saturation equation and because of this, each equation can be solved independently for its own variable. For a given saturation field at time level n, after assembling of Eq. (5) for all control volumes in the grid, a linear system of equations for the nodal values of pressure is obtained. Solving this system, the corresponding discrete pressure field for time level n can be determined and, consequently, total velocities at integration points $(\vec{\mathbf{v}}_T)_i^n$ can be computed using Eq. (3). Finally, saturation can be advanced to the next time level solving Eq. (4) for s_p^{n+1} at each node in the grid. The whole transient solution for a two-phase displacement problem can be obtained repeating iteratively the basic steps outlined above.

At this point nothing has been stated yet about the spatial interpolation schemes needed for relating integration point values to nodal values in Eqs. (4) and (5). Saturation equation is a nonlinear hyperbolic equation [14] and, consequently, if we consider a non monotonicity-preserving scheme, a formulation prone to develop spurious oscillations could be obtained. Therefore, the flux-corrected transport strategy will be used for approximating the advection term in Eq. (4), as described in the following section. Pressure equation, on the other hand, is an elliptic equation and a second-order scheme, like bilinear interpolation, can be used safely for expressing integration point values of pressure gradient and total mobility as a function of corresponding nodal values. This is the approach considered in this work for the pressure equation. More details about that can be found in references [8] and [13].

3. THE FLUX-CORRECTED TRANSPORT STRATEGY

In this section, the flux-corrected transport strategy will be applied to the saturation equation, Eq. (4), of the two-phase model flow outlined in the previous section. The application of FCT requires four main ingredients [10]:

1. A *low-order* discretization of the differential equation that renders a monotonic solution, without overshoots and undershoots but maybe with a strong extent of numerical diffusion.
2. A *high-order* discretization of the same equation.
3. *Antidiffusive fluxes*, defined as the difference between fluxes in the high-order discretization and fluxes in the low-order discretization. If those antidiffusive fluxes were added to the low-order solution, the high-order solution would be recovered. This solution, however, would be prone to develop oscillations near discontinuities.
4. *Flux limiters* reducing antidiffussive fluxes to the maximum extent possible without introducing oscillations and unphysical values into the solution.

Equation (4) can be rewritten as

$$(s_p^{n+1} - s_p^n)\,\frac{\phi_p \Delta V_p}{\Delta t} = -\sum_e \left\{ \sum_i (f)_i^n \right\}_e , \tag{6}$$

where $(f)_i^n$ are the fluxes across the faces between the given control volume and its neighbors, namely

$$(f)_i^n = F_i^n (\vec{\mathbf{v}}_T)_i^n \cdot \Delta\vec{\mathbf{S}}_i . \tag{7}$$

Considering a given element, such as the one represented in Fig. 2, the interpolated fractional flux function at an integration point in a face inside that element can be expressed in general as

$$\left\{ F_i^n \right\}_e = [c]_i [F]_e^n , \tag{8}$$

where $[c]_i$ is a row-vector of weighting factors associated to the nodal values and $[F]_e^n$ is the column-vector of nodal values of the fractional flux function at time level n. Nodal values in $[F]_e^n$ are ordered according to the local numbering scheme shown in Fig. 2.

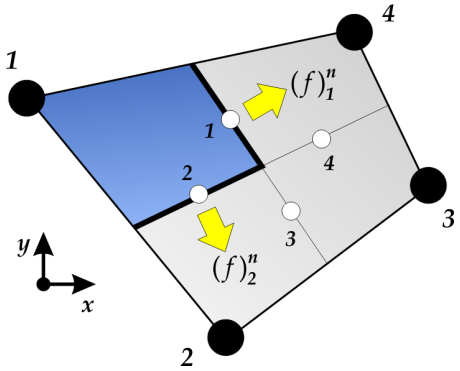

Figure 2 – Fluxes across the faces of a control sub-volume inside and element.
The local numbering of nodes and integration points is also shown.

If the vector of weighting factors in Eq. (8) corresponds to a low-order interpolation scheme, the low-order fluxes would be defined as

$$\left\{ (f_L)_i^n \right\}_e = \left\{ (\vec{\mathbf{v}}_T)_i^n \cdot \Delta\vec{\mathbf{S}}_i \, [c_L]_i \right\}_e [F]_e^n . \tag{9}$$

On the other hand, high-order fluxes would obtained if weighting factors correspond to a high-order scheme

$$\left\{ (f_H)_i^n \right\}_e = \left\{ (\vec{\mathbf{v}}_T)_i^n \cdot \Delta\vec{\mathbf{S}}_i \, [c_H]_i \right\}_e [F]_e^n . \tag{10}$$

In our implementation, the single-point upwind scheme was utilized as low-order scheme. The weighting factors for this scheme are the simplest possible and are defined by expressions of the type

$$[c_L]_1 = \begin{cases} [1 \quad 0 \quad 0 \quad 0] & \text{if } (\vec{\mathbf{v}}_T)_1^n \text{ points to node 4} \\ [0 \quad 0 \quad 0 \quad 1] & \text{if } (\vec{\mathbf{v}}_T)_1^n \text{ points to node 1} \end{cases}, \tag{11}$$

which is valid for integration point 1, according to the numbering scheme shown in Fig. 2. Equivalent expressions for other integration points can be easily obtained considering that, according to the scheme, the value at an integration point is equal to the value of the nearest upstream node.

As high-order scheme it was considered a bilinear interpolation, which is formally second-order [16]. With this choice, weighting factors in $[c_H]_i$ are equal to the values of bilinear shape functions [13] at integration points. For instance, at integration point 1 we have,

$$[c_H]_1 = \left[\frac{3}{8} \quad \frac{1}{8} \quad \frac{1}{8} \quad \frac{3}{8} \right]. \tag{12}$$

The antidiffusive fluxes can be introduced now as

$$\left\{ a_i^n \right\}_e = -\left[\left\{ (f_H)_i^n \right\}_e - \left\{ (f_L)_i^n \right\}_e \right]. \tag{13}$$

At this stage, the most essential component of FCT, namely the flux limiters, must be defined. In order to do this, an intermediate solution for saturation must be obtained employing the low-order scheme

$$\tilde{s}_p = s_p^n - \frac{\Delta t}{\phi_p \Delta V_p} \sum_e \left\{ \sum_i (f_L)_i^n \right\}_e \tag{14}$$

Flux limiters in FCT are designed in a way that a local maximum in the solution cannot increase and a local minimum cannot decrease. A scheme that possesses this property is said to be local extremum diminishing (LED) [10] [11]. It guarantees positivity, because if a numerical solution is positive everywhere at certain stage, it will remain positive all the time since the global minimum cannot decrease and consequently it cannot get negative values. The LED property precludes also the birth and growing of spurious oscillations [11].

In order to guarantee that limited antidiffusive fluxes satisfy the LED criterion, local upper and lower bounds for the nodal saturation values must be stated. These bounds can be determined searching the local minimum / maximum values of the intermediate solution given by Eq. (14), in the following way

$$\tilde{s}_p^{\min}{}^{\max} = \min^{\max}\left(\tilde{s}_k \right), \quad k \in \mathsf{S}_p, \tag{15}$$

where S_p is the set of nodes in the stencil associated to node p, or in other words, the set of nodes at the vertices of all elements sharing the node p.

After calculating the upper and lower bounds for each nodal value of saturation, the maximum admissible increment and decrement in relation to the intermediate solution can be computed,

$$Q_p^{\pm} = \tilde{s}_p^{\min}{}^{\max} - \tilde{s}_p. \tag{16}$$

Since the increment of nodal values of saturation is caused by positive antidiffusive fluxes and decrement is caused by negative ones, these effects can be examined separately. In order to

do this, other two sets of auxiliary quantities must be defined. These are the sum of all positive / negative antidiffusive fluxes associated to each control volume,

$$P_p^{\pm} = \sum_e \left\{ \sum_i \begin{matrix} \max \\ \min \end{matrix} \left(0, a_i^n\right) \right\}_e . \tag{17}$$

In order to prevent the creation of new local extrema, the positive / negative antidiffusive flux $\left\{ a_i^n \right\}_e$ should be multiplied by [10]

$$R_p^{\pm} = \begin{cases} \min\left(1, Q_p^{\pm}/P_p^{\pm}\right), & if\ P_p^{\pm} \neq 0 \\ 1, & if\ P_p^{\pm} = 0 \end{cases}, \tag{18}$$

However, since an antidiffusive flux influences nodal values from two neighbor control volumes (a positive flux for a given control volume is negative for its neighbor and vice versa), the minimum of the two correction factors should be kept, according to the sign of the flux [10],

$$\left\{ \beta_i \right\}_e = \begin{cases} \min\left(R_p^+, R_m^-\right), & if\ \left\{ a_i^n \right\}_e \geq 0 \\ \min\left(R_m^+, R_p^-\right), & if\ \left\{ a_i^n \right\}_e < 0 \end{cases}. \tag{19}$$

In this equation, p and m are the nodes associated to two control volumes sharing the face where integration point i is located, as depicted in Fig. 3.

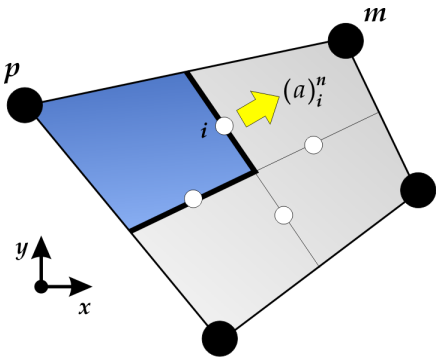

Figure 3 – Neighbor nodes for a given integration point inside an element.

After completing the sequence of calculations sketched above, the flux limiters will be ready for using in the calculation of the final solution for the saturation at time level $n+1$. This solution for every node is given by

$$s_p^{n+1} = \tilde{s}_p + \frac{\Delta t}{\phi_p \Delta V_p} \sum_e \left\{ \sum_i \beta_i a_i^n \right\}_e \tag{20}$$

Since flux limiters were designed to satisfy the LED criterion, the discrete approximation of the saturation field computed with Eq. (20) will be monotonic, always positive and free of overshoots / undershoots. Despite the fact that the inclusion of FCT requires some extra steps in the IMPES algorithm outlined in section 2, such as the computation of antidiffusive fluxes, the computation of an intermediate solution for saturation and the computation of flux limiters, those steps are in general considerably less time-demanding than the solution of the linear for the pressure. But this a little price for obtaining much sharper fronts in the numerical solutions. Numerical experiments show that the front thickness in numerical solutions obtained employing FCT are approximately half of the thickness in a solution without FCT. Some results showing this are presented in the following section.

4. APPLICATION EXAMPLES

As first example, a quarter of the five-spot configuration [18] [19] was considered for simulating a waterflood. In general, the solution for the saturation field is a compound by a shock and a rarefaction [1]. The most demanding test for our formulation would be a situation where only a shock with the maximum strength possible exists, the so-called piston-type displacement [19]. This situation can be modeled prescribing, for instance

$$F(s) = s \tag{21}$$

$$\hat{\lambda}_T(s) = \frac{M}{M - (M - 1)\, s} \tag{22}$$

where $\hat{\lambda}_T$ is the total mobility normalized by the maximum value of the oil mobility, whereas M is the ratio of the maximum water mobility to the maximum oil mobility.

Two grids were considered for this test, a Cartesian one and a non-orthogonal unstructured one, as depicted in Fig. 4. An injection well is located in the lower left node of each grid, whereas a production well is placed at the upper right node. A constant volumetric flow-rate of water is injected through the injection well.

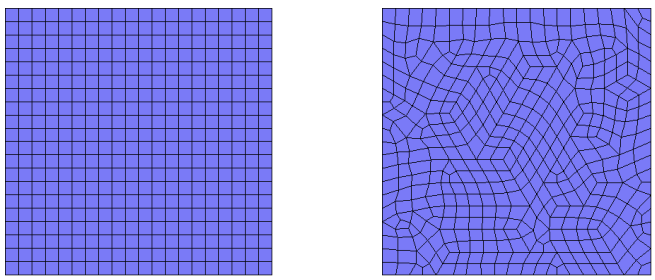

(a) (b)

Figure 4 – (a) Cartesian 20×20-element grid and (b) unstructured 440-element grid, used for discretizing a quarter of the five-spot configuration.

Figure 5 shows four snapshots of the time evolution of the water-oil front, corresponding to four numerical solutions of the five-spot problem sketched above. The fractional flux function and total mobility were set according Eqs. (21) and (22), with a mobility ratio $M = 2.5$ in all cases. The first two rows compares the solutions obtained with the 20×20-element Cartesian grid, one using the basic formulation without FCT whereas the other using the formulation including the FCT strategy described in section 3. An equivalent comparison is made in the third and fourth

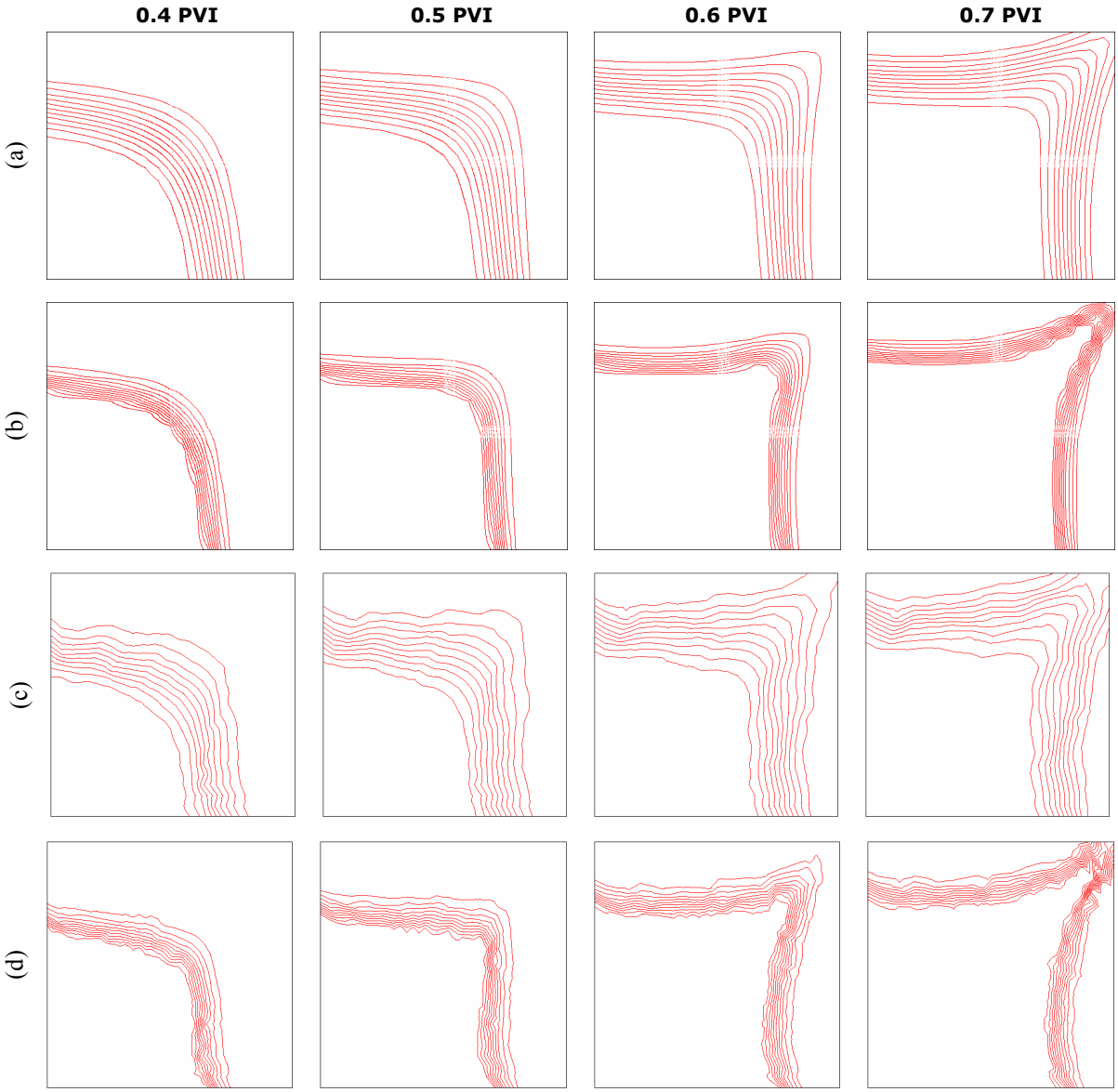

Figure 5 – Saturation isolines at four time levels of the solution of the five-spot problem obtained (a) without FCT and (b) with FCT, in the Cartesian 20×20-element grid; (c) without FCT and (d) with FCT in the unstructured 440-element grid.

rows, which correspond to solutions obtained with the 440-element unstructured grid, again one without FCT and the other with FCT. Both comparisons demonstrate clearly that a significant amount of numerical diffusion has been removed by the application of the FCT strategy. The thickness of the front in the solution with FCT is roughly the half of the thickness in the solution with the basic formulation. This behavior is observed in both grids, the regular Cartesian and the irregular unstructured, in fairly the same manner.

As second example, a water-oil displacement in a reservoir with a more complex geometry is considered. The quadrilateral unstructured grid utilized in the simulation is depicted in Fig, 6. Local refinement is considered in regions around wells (one injection well and two production wells) since usually more accurate solutions are required in those regions. This is one of the main advantages of using unstructured grids, because small elements can be concentrated only in localized interesting areas without increasing excessively the size of the whole discrete problem. Moreover, with unstructured grids, the transition between refined and coarse regions can be made smoothly, in order to avoid introducing further discretization errors associated to element sizes varying abruptly. A geological fault also present into the considered reservoir was modeled as an internal impervious boundary. The grid was enforced to conforming to the domain boundary, modeled also as an impermeable boundary, as well as the internal fault.

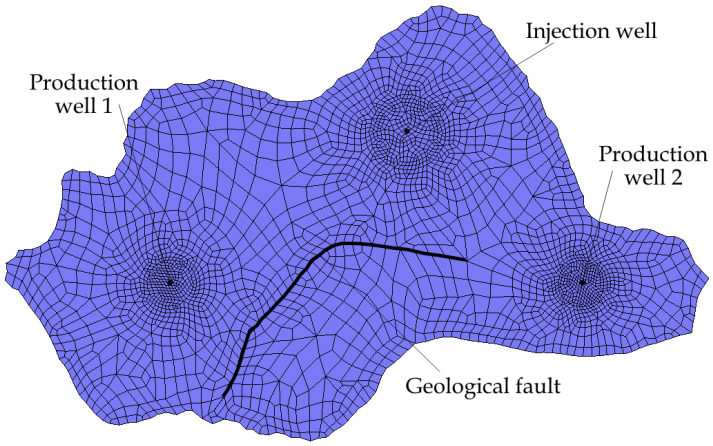

Figure 6 – Unstructured grid for a reservoir considered in the second example.

Results of simulations performed with the same fractional flow function and total mobility as the previous example are shown in Figs. 7 and 8. These figures shown again two solutions, one obtained without considering FCT and other including it in the formulation. As can be seen, once more an enhancement in the sharpness of the front is evident in the solution with FCT. Although in this case the thickness of the front differs from one region to another due to the variability of the element size in the grid, the front is clearly thicker in the solution without FCT. This example demonstrates that the formulation including FCT is proficient in reducing numerical diffusion in fully unstructured grids discretizing complex geometries.

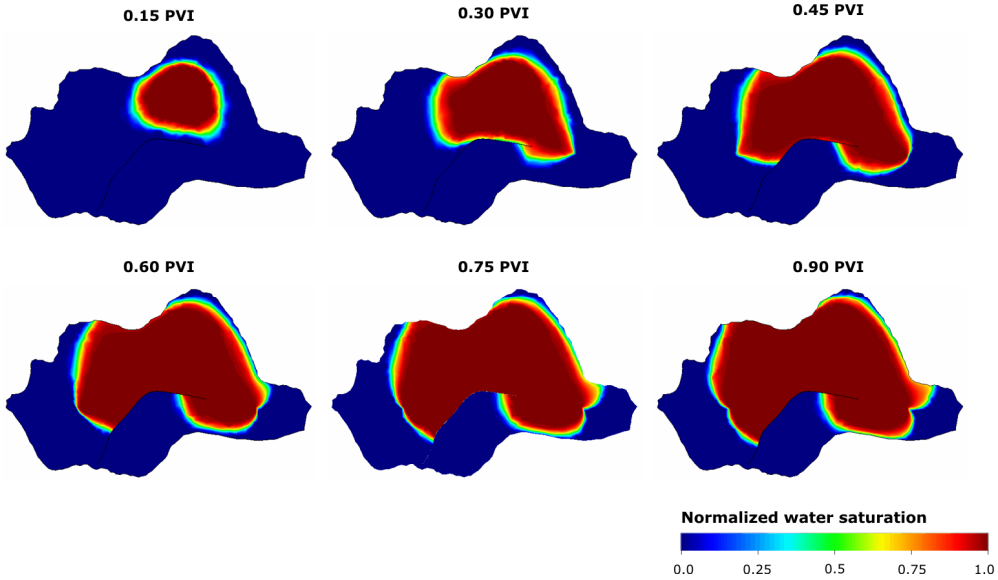

Figure 7 – Evolution of the normalized saturation field obtained with the basic formulation without FCT.

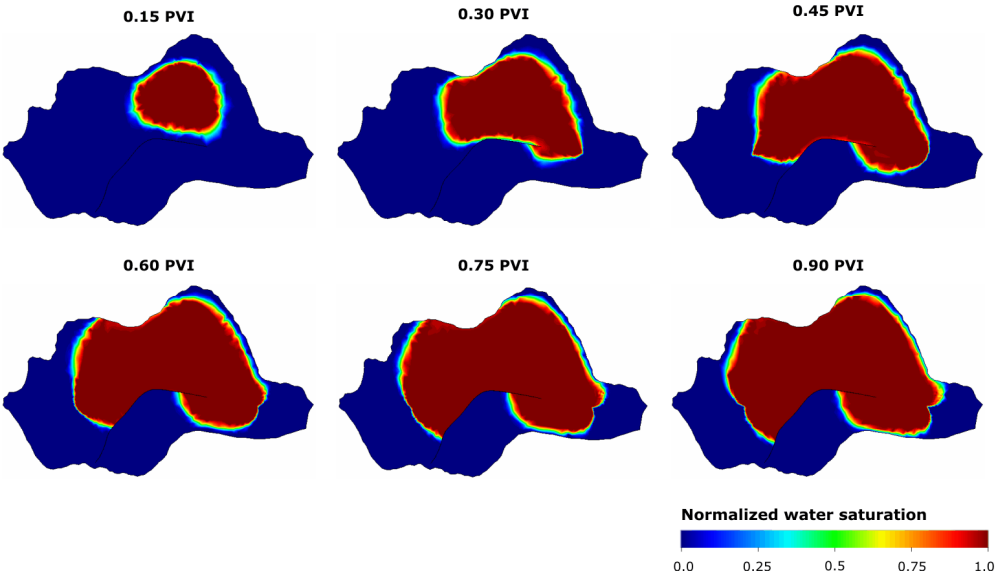

Figure 8 – Evolution of the normalized saturation field obtained with the formulation including FCT.

5. CONCLUDING REMARKS

In this work, the flux-corrected transport (FCT) strategy has been applied to a finite-volume unstructured-grid formulation for reservoir simulation. The application examples presented shown that FCT is an effective technique for reducing numerical diffusion in numerical simulation, preventing at the same time the birth and growing of spurious oscillations. The approach

considered in this work for implementing FCT is rather simple and fairly increases the computational effort for solving the whole set of discretized equations employing the IMPES algorithm. Future works must address the extension of the methodology to the fully implicit approach. Some authors have been shown that this extension is feasible for models like the Euler equations for compressible flow.

ACKNOWLEGEMENTS

The first author acknowledges financial support of Agência Nacional do Petróleo (ANP) through a scholarship.

REFERENCES

[1] Allen, M. B., Behie, G. A., Trangenstein, J. A. *Multiphase flow in porous media, mechanics, mathematics and numerics*. Lecture Notes in Engineering Series, Vol. 34. Springer Verlag, Berlin, Germany, (1988).

[2] Aziz, K., Settari, A. *Petroleum reservoir simulation*. Applied Science Publishers Ltd., London, England, (1979).

[3] Bell, J. B., Shubin, G. R. "High-order Godunov methods for reducing numerical dispersion". *Paper SPE 13514, Reservoir Simulation Symposium*, Dallas, USA, February 10-13, (1985).

[4] Carr, A. H., Christie, M. A. "Controlling numerical diffusion in reservoir simulation using flux corrected transport". *Paper SPE 12235, Reservoir Simulation Symposium,* San Francisco, USA, November 15-18, (1983).

[5] Christie, M. A., Bond, D. J. "Multidimensional flux-corrected transport for reservoir simulation". *Paper SPE 13505*, *Middle East Oil Technical Conference*, Bahrain, March 11-14, (1985).

[6] Ferziger, J. H., Perić, M. *Computational methods for fluid dynamics.* Second edition, Springer Verlag, Berlin, Germany, (1998).

[7] Hirsch, C. *Numerical computation of internal and external flows.* Vol. 2. John Wiley and Sons, Chichester, England, (1990).

[8] Hurtado, F. S. V. *An element-based finite volume formulation for the simulation of two-phase immiscible flow in porous media*. M.Sc. Dissertation (in Portuguese), Mechanical Engineering Department, Federal University of Santa Catarina, Brazil, (2005).

[9] Hurtado, F. S. V., Maliska, C. R., Silva, A. F. C., Cordazzo, J. "An element-based finite volume formulation for reservoir simulation". *Proceedings of the XXVI Iberian Latin-American Congress on Computational Methods in Engineering* – CILAMCE 2005, Gurarpari/ES, Brazil, October 19-21, (2005).

[10] Kuzmin, D., Löhner, R., Turek, S. *Flux-corrrected transport*. Springer Verlag, Berlin,

Germany, (2005).

[11] Kuzmin, D., Möller, M., Turek, S. "High-resolution FEM-FCT schemes for multidimensional conservation laws". *Int. J. Numer. Meth. Fluids,* Vol. 42, pp. 265-295, (2003).

[12] Löhner, R. *Applied computational fluid dynamics techniques*. John Wiley & Sons, Ltd, Chichester, England, (2001).

[13] Maliska, C. R. *Transferência de calor e mecânica dos fluidos computacional*, 2ª edição revista e ampliada. Livros Técnicos e Científicos Editora S. A., Rio de Janeiro, Brasil, (2004).

[14] Peaceman, D. W. *Fundamentals of numerical reservoir simulation.* Developments in Petroleum Science Series, Vol. 6, Elsevier Scientific Publishing Company, (1977).

[15] Pinto, A. C. C., Correa, A. C. F., Cunha, M. C. C. "High-resolution schemes for conservation laws: application to reservoir engineering". *SPE Paper 24262, SPE European Petroleum Computer Conference,* Stavenger, Norway, May 25-27, (1992).

[16] Raw, M. J. *A new control-volume-based finite element procedure for the numerical solution of the fluid flow and scalar transport equations*. Ph.D. Thesis, University of Waterloo, Canada, (1985).

[17] Rubin, B., Blunt, M. J. "Higher-order implicit flux limiting schemes for black oil simulation". *SPE Paper 21222, 11th Symposium of Reservoir Simulation*, Anahein, USA, February 17-20, (1991).

[18] Todd, M. R., O'Dell, P. M., Hirasaki, G. J. "Methods for increased accuracy in numerical reservoir simulators". *SPE Journal*, Vol. 12, pp. 515-530, (1972).

[19] Yanosik, J. L., McCracken, T. A. "A nine-point finite difference reservoir simulator for realistic prediction of adverse mobility ratio displacements". *SPE Journal,* Vol. August 1979, pp. 253-262, (1979).